Computational Fluid Dynamics Coupled with Thermal Impact Model for Building Design

Sue Ellen Haupt[1,2], Robert F. Kunz[1,3], L. Joel Peltier[1,4], James J. Dreyer[1]

[1] The Pennsylvania State University/Applied Research Laboratory, State College, PA, USA

[2] The Pennsylvania State University/Meteorology Department, University Park, PA, USA

[3] The Pennsylvania State University/Aerospace Engineering Department, University Park, PA, USA

[4] Bechtel Corporation, Frederick, MD, USA (current affiliation)

Email: seh19@psu.edu; rfk102@arl.psu.edu; ljpeltie@bechtel.com; jjd5@arl.psu.edu

***Abstract*— Thermal effects impact the flow around and within structures. This computational study assesses features that affect the heating and buoyancy, and thus, the resulting flow both internal and external to a building. Considerations include the importance of time of day, building materials, sky cover, etc. on the local thermal heating of a passive solar building. Such impacts are assessed using full thermal coupling between a building energy simulation model and a computational fluid dynamics model, including the effects of thermal radiation, conduction, and convection to analyze the impact of all natural heating, cooling, and flow mechanisms for both the interior and exterior. Unique features such as Trombe walls add to heat transfer mechanisms. Analysis is made for three separate seasonal conditions.**

***Index Terms*— Building Energy Simulation, Building Design, Thermal Modeling, Computational Fluid Dynamics, Trombe Walls**

I. Introduction

Design of modern energy efficient buildings often involves modeling both air flow and the efficiency of heat transfer mechanisms. Computational fluid dynamics (CFD) has become a recognized method of assessing air flow, heat transfer, and contaminant transport both inside and outside buildings during the design phase [1], [2]. Likewise, energy transfer mechanisms are often simulated using building energy simulation (BES) models [3]. Recent studies have demonstrated the utility of coupling BES models with CFD simulations. [4],[5],[6],[7],[8],[9],[10],[11],[12], and [13].

Yamada [14] has recently shown temperature variations between urban and rural areas in a CFD model that includes thermal energy balances. Huang, et al. [15] developed a numerical simulation program incorporating convection, radiation, and conduction including a three dimensional CFD model. They modeled the influence of heat released from rooftops and conjectured about the resulting influence on atmospheric dispersion. Dispersion around multiple buildings computed via CFD was compared with that produced by an atmospheric transport and dispersion Lagrangian puff model by Long et al [16].

The purpose of this current study is to model the impact of all types of heat transfer – radiation, conduction, and convection – on the flow interior and immediately exterior to a building. This paper reports on coupling a building energy simulation model with a high fidelity CFD model to analyze passive solar heat transfer mechanisms and natural ventilation. Passive solar features such as Trombe walls and large glassed areas are studied. Four heating cases are modeled that represent disparate heating conditions: 1) summer, 2) fall transition, 3) winter, and 4) no heating.

Section 2 describes the modeling approach, focusing on coupling the BES and CFD models. Section 3 describes the results by analyzing fluid flow, heat transfer, and mean radiant heating. A discussion and recommendations for further study appear in section 4.

II. Modeling Approach

A. The Building

The building modeled has an environmentally-friendly design and is shown in Figure 1. Figure 1a is a front view while 1b and 1c look into the upper and lower levels of the building respectively. The building emphasizes passive solar features, including Trombe walls for heat transfer. Those walls are glass on the exterior, with a six inch open air space in front of a masonry wall. Solar radiation heats the wall, which transfers its heat to the air between the glass and the back wall. As the warmer air rises in the open space and is vented into the building via duct openings, it is replaced by cooler air from below via three air ducts on the interior wall. This passive solar heating from the Trombe walls, as well as through the large glass front windows, reduces the need for mechanical heating in winter. The long awnings, however, prevent excessive summer heating when the solar zenith angle is higher. The goal of this study is to assess the effectiveness of these passive solar heating mechanisms using state-of-the-art modeling tools.

doi:10.4304/jcp.5.10.1552-1559

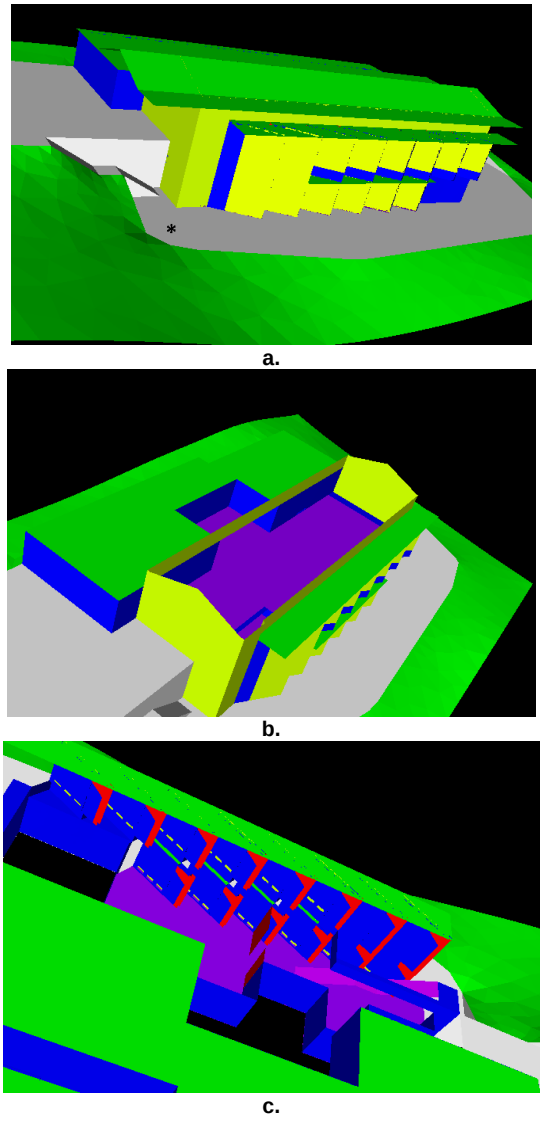

Figure 1. Geometry of the building modeled. a. exterior view indicating Trombe walls, b. view of upper level from above with roof removed, and c. view of lower level and inside view of Trombe walls.

B. The Grid

A computational grid was constructed inside and outside of the building (including the terrain) using the commercially available grid generation software, GRIDGEN. The mesh is constructed with higher resolution adjacent to and within the Trombe walls (where significant velocity gradients arise due to free convection,) and, in general, adjacent to all solid boundaries to adequately resolve the developing turbulent boundary layers. A total of approximately 2.1 million tetrahedral elements are used in the mesh. The mesh appears in Figure 2. Figure 2a shows the surface mesh over the building and terrain and 2b is a cut plane of the mesh taken through the building. Note the high density of the mesh in the vicinity of the Trombe walls where a significant thermal circulation is expected to develop.

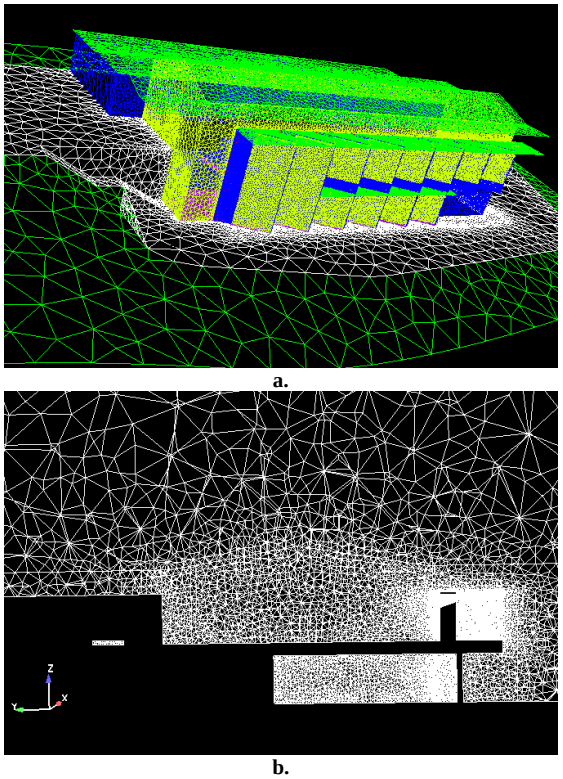

Figure 2. Building mesh. a. Exterior mesh indicating finer grid spacing close to building. b. mesh inside building is finer, especially in the small spaces of the Trombe walls.

C. The CFD Model

The governing equations for the flow field are the compressible continuity, momentum and energy equations:

$$\frac{\partial}{\partial x_j}\left(\rho u_j\right) = 0 \ , \tag{1}$$

$$\frac{\partial}{\partial x_j}\left(\rho u_j u_i\right) = -\frac{\partial p}{\partial x_i} + \frac{\partial}{\partial x_j}\tau_{ij} + \rho g_i \ , \tag{2}$$

$$\frac{\partial}{\partial x_j}\left(\rho u_j h\right) = u_j\frac{\partial p}{\partial x_j} + \tau_{ij}\frac{\partial u_i}{\partial x_j} - \frac{\partial q_j}{\partial x_j} \ . \tag{3}$$

with shear stress tensor and heat flux vector defined as:

$$\tau_{ij} \equiv \left[\left(\mu+\mu_t\right)\left(\frac{\partial u_i}{\partial x_j}+\frac{\partial u_j}{\partial x_i}\right)\right], q_j \equiv -\left[\left(\frac{\mu}{\sigma}+\frac{\mu_t}{\sigma_{t,h}}\right)\left(\frac{\partial h}{\partial x_j}\right)\right] \tag{4}$$

In equations (1-3), ρ, u_j, p, g_i, h *and* x_j are the density, velocity vector, static pressure, gravity vector, static enthalpy and Cartesian coordinate vector respectively. Taking the air in this system as a calorically perfect gas, temperature and density are obtained from $h = C_P T$, $p = \rho RT$ with $\gamma = 1.4$, $R = 287\ J/kg*K$ for air, and $C_P = \gamma R/\left(\gamma\text{-}1\right)$. In the shear stress and heat flux

relations, an appropriate molecular viscosity, μ = 1.0x10^{-5} kg/m*s was specified for air. Likewise, in the heat flux expression, an appropriate Prandtl number, σ =0.72 was specified.

An eddy viscosity formulation is employed to model the effects of turbulence, with closure in (2) and (3) provided by the standard k-ε turbulence model:

$$\frac{\partial}{\partial t}(\rho k)+\frac{\partial}{\partial x_j}(\rho u_j k)=\frac{\partial}{\partial x_j}\left[\left(\mu+\frac{\mu_t}{\sigma_{t,k}}\right)\frac{\partial k}{\partial x_j}\right]+P-\rho\varepsilon \quad (5)$$

$$\frac{\partial}{\partial t}(\rho\varepsilon)+\frac{\partial}{\partial x_j}(\rho u_j \varepsilon)=\frac{\partial}{\partial x_j}\left[\left(\mu+\frac{\mu_t}{\sigma_{t,\varepsilon}}\right)\frac{\partial \varepsilon}{\partial x_j}\right]+C_1\frac{\varepsilon}{k}P-C_2\frac{\varepsilon}{k}\rho\varepsilon \quad (6)$$

In (5) and (6), k, ε, C_1, C_2 are the turbulent kinetic energy, the turbulent dissipation rate, and model constants, C_1=1.44, C_2=1.92. The turbulence production rate, P is given in this model by the Boussinesq assumption:

$$P\equiv\frac{\partial u_i}{\partial x_j}\left[\mu_t\left(\frac{\partial u_i}{\partial x_j}+\frac{\partial u_j}{\partial x_i}\right)\right] \quad (7)$$

The eddy-viscosity is defined from the Prandtl-Kolmogorov relation:

$$\mu_t\equiv\frac{C_\mu k^{3/2}}{\varepsilon} \quad (8)$$

with additional model closure constants: C_μ=.09, σ_t=0.91, $\sigma_{t,k}$=1.00, $\sigma_{t,\varepsilon}$=1.30.

The CFD code used here, NPHASE-PSU, is three-dimensional, supports unstructured grids, and is parallelized. The baseline algorithm follows a segregated pressure based methodology. A colocated variable arrangement is used and a lagged coefficient linearization is applied. One of several diagonal dominance preserving, face-based finite volume spatial discretization schemes is selected for the momentum and turbulence transport equations. Continuity is introduced through a pressure correction equation, based on the SIMPLE-C algorithm [17],[18],[19],[20]. At each iteration, the discrete momentum equations are solved approximately, followed by a more exact solution of the pressure correction equation, followed by an approximate solution of the enthalpy equation.

D. The Heat Transfer Model

The conduction and radiation physics of the coupled model is provided by the commercial software package, RadTherm [21]. RadTherm carries out transient thermal analysis that includes the effects of conduction, radiation, and wall heat convection. Conduction heat transfer is primarily dependent on material properties and local material thickness (user specified for each surface/material) in the direction of the local temperature gradient. Radiation heat transfer depends on surface properties (user specified for each surface/material) and view factors (computed by RadTherm). Both conduction and radiation physics are important in this problem, but are fundamentally uncoupled from the flow. Convection heat transfer is strongly coupled to the flow field and is therefore where the coupling between RadTherm and NPHASE-PSU is required. Specifically, convection heat transfer is modeled in RadTherm using heat transfer coefficients and film temperatures provided by NPHASE-PSU, as detailed below.

Important in these simulations, Radtherm also includes extensive utilities for modeling environmental factors including the effects of:

- solar radiation as a function of the position of sun and atmospheric conditions provided by an external weather file,
- full shadowing based on time of day, geometry, and reflections,
- re-radiation between geometric features,
- glass regions that are transparent to solar radiation but opaque to infrared radiation,
- sky radiation.

RadTherm uses ray tracing to compute radiation view factors and solar projected (apparent) areas.

E. Environmental Conditions

Three separate days of the year are modeled. Complete diurnal cycles are run for a representative warm summer day, a cold winter day, and a day in early autumn. Sunny days were chosen to model the maximum impact of the time-dependent solar radiation forcing function. Total solar energy flux, relative humidity, and cloud cover are time-dependent weather metrics that are provided by an external weather data file. The source of the weather data used in RadTherm for the diurnal thermal analyses is the Typical Meteorological Year (TMY2) dataset produced by the Analytic Studies Division of the National Renewable Energy Laboratory [22]. The diurnal cycle of temperature, humidity, and solar radiation for the December case is shown in Figure 3. A fourth control case was run that does not include any heating effects.

Within RadTherm, the character of the incident solar energy is determined by the total solar energy flux, the altitude above sea level, the relative humidity, the amount of cloud cover, and the global position and orientation of the building. The latter are fixed geometric properties of the structure that determine the directivity of the radiation and shadowing.

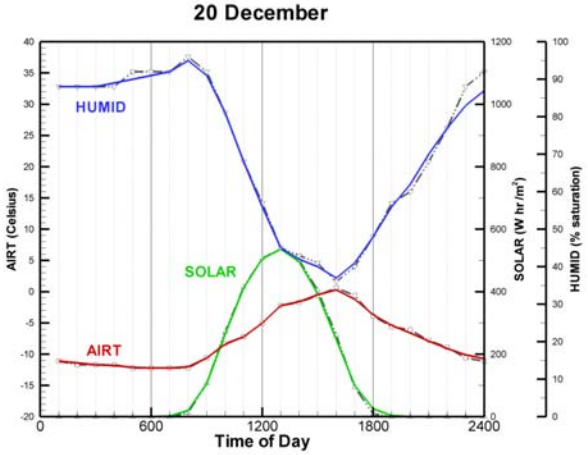

Figure 3. The diurnal variation of air temperature, solar radiation, and relative humidity that is used as input for the coupled modeling system for the December case.

Figure 4 shows how the solar radiation impacts temperatures on the exterior building walls at different times of day for the early autumn day. Much of the building is cool during the night hours except for around the patio and some areas of the Trombe walls that have retained heat from the prior day's heating. Radiative heating from the sun becomes evident by 0800 and progresses at 1000. Figure 4d shows the shadowing effects that occur mid-day on the Trombe walls by the overhanging awnings. The patio and walls are heated by mid-afternoon and begin to cool by 1800 as indicated in Figure 4f. Low external wind speeds are used (1m/s) to minimize forced convection effects and maximize the free convection buoyancy effects on the heating and cooling of the building.

F. Iterative Solution

A complete diurnal simulation of the heating and cooling of the structure coupled with the (primarily) thermally-driven fluid flow inside and outside the structure is obtained by loosely coupling RadTherm and NPHASE-PSU (see Figure 5). The coupling mechanism is implemented as follows: The flow field is updated six times (00:00, 08:00, 10:00, 13:00, 16:00, and 18:00) in a 24 hour period using steady-state flow solutions computed by NPHASE-PSU, using instantaneous wall temperatures provided by RadTherm. These six times are chosen at non-uniform increments (between 2 and 8 hours) to better resolve the most transient portions of the day, e.g., early morning and late afternoon.

RadTherm is then run through a complete 24 hour cycle using local convective heat transfer coefficients, H, and fluid film (adjacent to wall) temperatures, T_{film}, interpolated in time from the six NPHASE-PSU steady solutions. The time-dependent environmental forcing provided by the weather file and the material and surface properties of the building elements are critical to the heating analysis. This diurnal analysis is repeated with NPHASE-PSU providing H and T_{film} to the proceeding RadTherm run and RadTherm providing T_{wall} to the proceeding NPHASE-PSU run, until two consecutive diurnal cycles are effectively indistinguishable by two criteria: 1) wall temperatures vary by less than ~1 °C, and 2) building internal air temperatures at 1 m above the

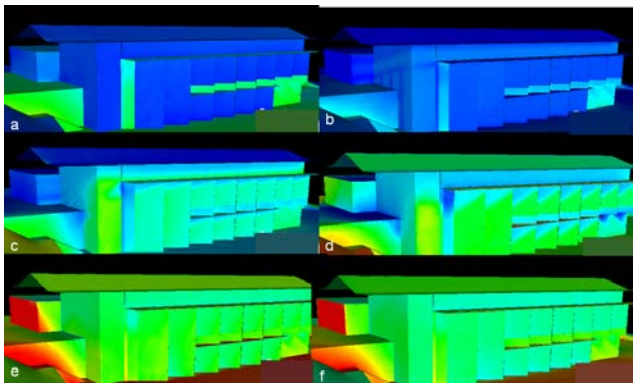

Figure 4. Temperature cycle on exterior walls of the building at 6 times of day for September case: a. 0000, b. 0800, c. 1000, d. 1300, e. 1600, and f. 1800.

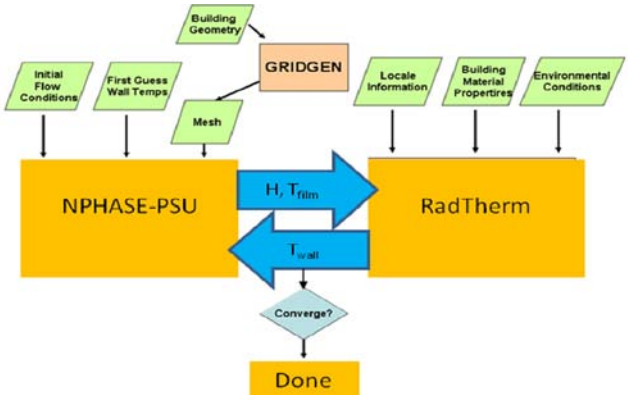

Figure 5. Flowchart of iterative heat transfer and flow solutions.

floor have converged to the same tolerance within NPHASE-PSU. This dual convergence typically requires between five and ten full cycles. It is this steady state solution at each of the six times for each of the three cases that is analyzed for differences in the flow field. Figure 6 shows how the solar angle, when taken together with the building geometry, can result in heating of an internal wall, which results in an elevated wall temperature at that time of day.

III. SIMULATION RESULTS

A. Thermally Driven Flow

1. Interior Flow

Fully three dimensional CFD was accomplished both the interior and the exterior of the building with full heating for the three heating cases. Figure 7 shows an isosurface of the temperature field inside the building for the winter case. The coloring is by velocity magnitude to enable visualization and to indicate the regions of maximum motion (warmer colors). The warmer air rises through the open spaces and settles in under the ceiling on the lower level and the roof on the upper level. This is evidence of rising motion within the second story Trombe wall as well as in the stairwell at the front of the building. A more detailed look at velocity vectors for the interior near the Trombe walls appears in Figure 8. It is apparent that warm air is vented out of the top of the Trombe walls. The heating from the floor is also evident in warmer temperatures near the floor as well as in the air from the Trombe walls.

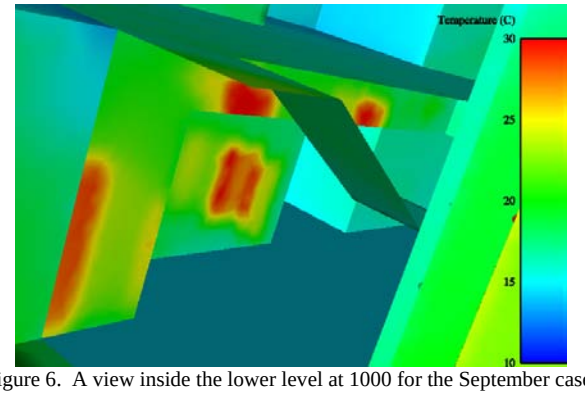

Figure 6. A view inside the lower level at 1000 for the September case. Heating on the back walls through the windows is evident.

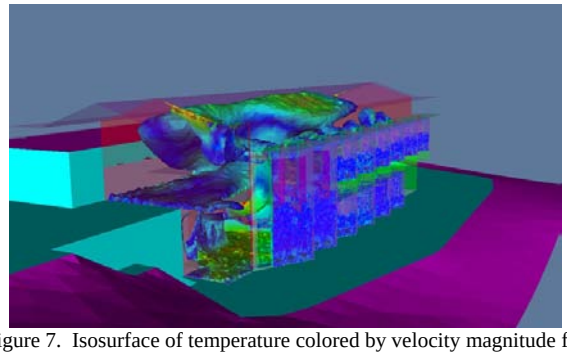

Figure 7. Isosurface of temperature colored by velocity magnitude for December heating case at 1600.

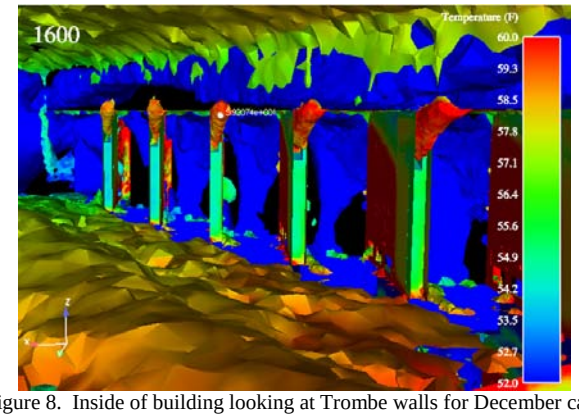

Figure 8. Inside of building looking at Trombe walls for December case at 1600. Isosurface of velocity magnitude is colored by temperature.

Figure 9 more closely examines the flow inside the Trombe walls via a velocity vector plot in that vicinity. Warmer air spreads out along the ceiling while the cooler air descends along the faces of the Trombe walls. It is obvious that warm air circulates upward both inside and outside the building. The Trombe walls vent the warmed air into the upper portion of each story of the building, creating a slow interior buoyancy-induced circulation zone. Note that velocities in this circulation remain less than 1 m/s.

2. Exterior Flow

The flow field exterior to the building is also influenced by the radiative heating. Figure 10 is a clip plane through the building perpendicular to the external wind field. It is colored by velocity magnitude for both the unheated (a) and heated (b) cases at 1600 for the winter day. The left portion of the two figures, along the

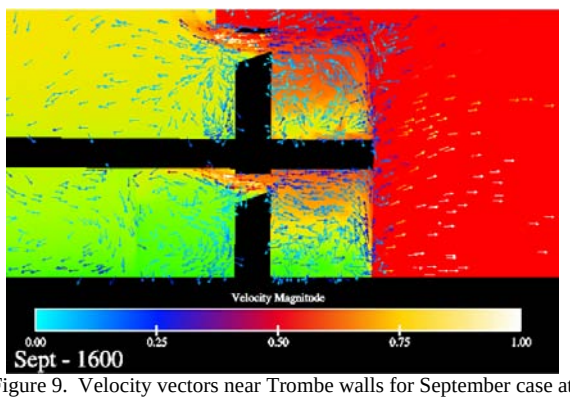

Figure 9. Velocity vectors near Trombe walls for September case at 1600.

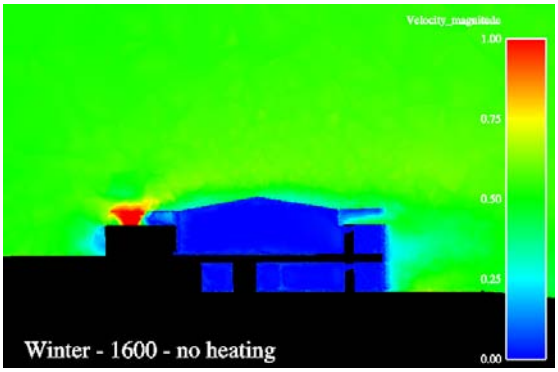

a.

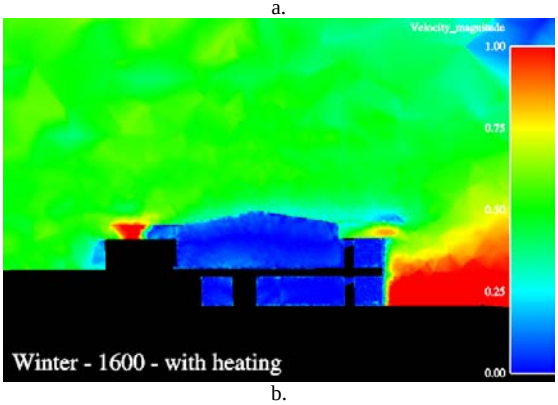

b.

Figure 10. Clip plane through the building colored by velocity magnitude. a. without heating, and b. with heating at 1600 for the winter case.

unheated storage section of the building show quite similar velocity plots, as expected, since no differential heating occurs there. The right side, however, is highly affected by the heating of the Trombe walls. When one breaks the velocity into its components, it is apparent that the change in the x-velocity (parallel to the Trombe walls) is the largest contributor to the differences. This observation is further elucidated by looking down onto a clip plane 5 m above the surface in Figure 11. The unheated case (a) indicates much slower velocities than the heated version (b). The along-building differences are primarily due to the x-velocity, but the differences behind the building are evident in plots of the z-velocity (not shown) where there are strong downdrafts in the lee of the building.

B. Heat Transfer Characteristics

The diurnal and seasonal differences in heating characteristics are evident upon analysis of the temperatures within the building. Figure 12 indicates the diurnal variation of the temperature computed 1 m above the floor for each of the heating cases. Several aspects of that plot confirm that the computations are appropriate. First, the temperatures are highest for the July case and lowest for the December case, in keeping with the external temperatures supplied as input for the model. Second, the temperatures are relatively constant early in the day (prior to sunrise), then increase gradually throughout the hours of solar heating. The heating progresses longest in July and shortest in December, as expected. Third, for all three cases, the temperatures are higher for the upper (main) floor than for the lower floor. Therefore, we are assured that the coupled models are computing the appropriate

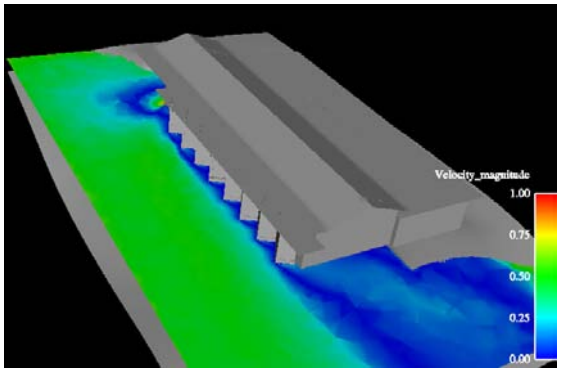

a.

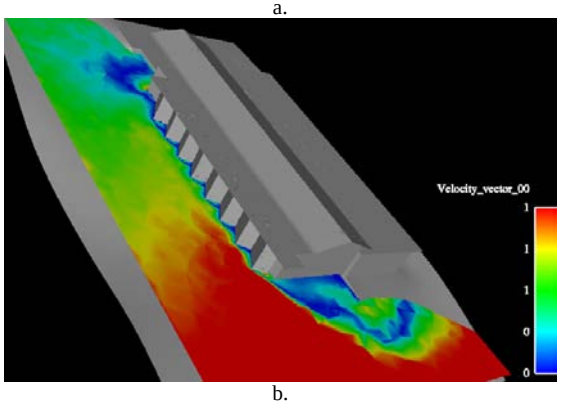

b.

Figure 11. Clip plane 5m above surface colored by velocity magnitude. a. without heating, b. winter case with heating at 1600.

temperature stratification throughout the building, given that there is no mechanical heating or forced convection included in these calculations. Note, however, that there is free convection between the upper and lower levels via the open stairwell and the two story open portion of the front of the building (Figure 1c).

Figure 13 shows the natural ventilation temperature stratification in the building for six different times in July, which is the case with the largest temperature difference throughout the building. The largest temperature differences from bottom to top of the

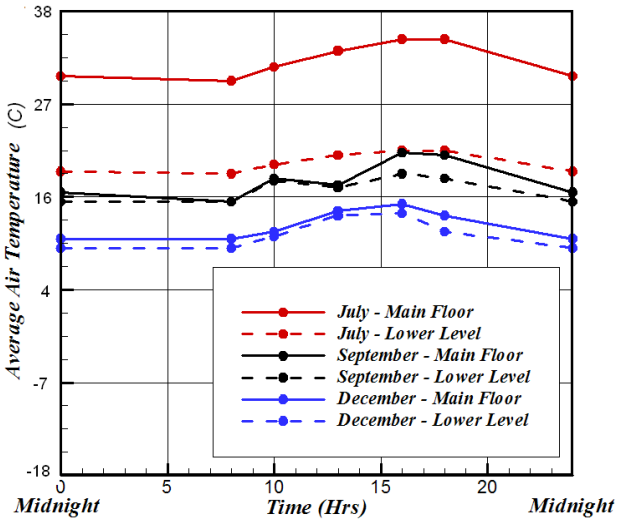

Figure 12. Diurnal temperature cycle of temperature as computed 1 m above the floor for both the upper (main) and lower level floor for each of the three heating cases.

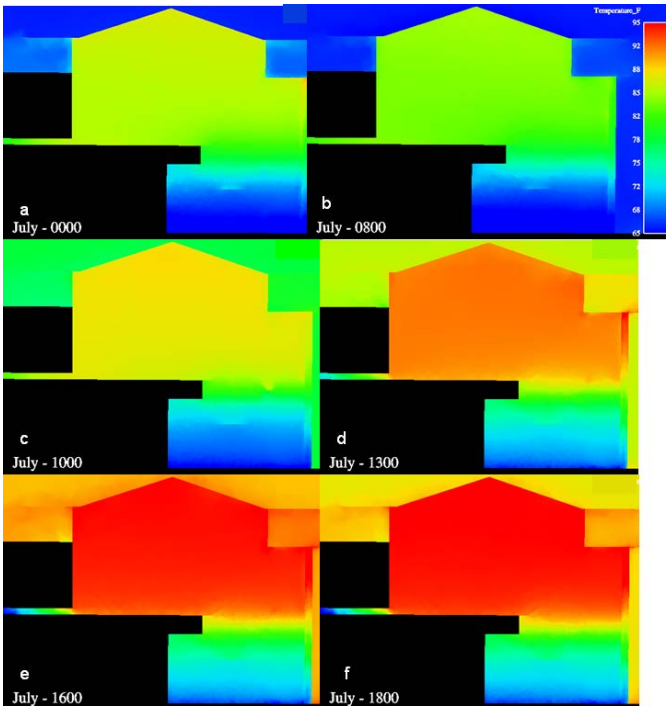

Figure 13. Clip plane colored by temperature through the building for six times in July.

building occur at 1800 after a full day of heating. Note that the large glass windows allow solar heating throughout much of the day. The building cools off over the nighttime hours (midnight-0000 and 0800 plots indicate continuous cooling). The 1000, 1300, and 1600 plots demonstrate gradual warming throughout the day results in increased stratification, in spite of the obvious communication between the levels via the stairwell.

C. Contaminant Dispersion

We additionally wish to model the dispersion of a contaminant released upstream of the building. We first assess the turbulent kinetic energy (TKE), which is an indicator of where dispersion differences may come into play. Figure 14 shows differences in TKE (computed as $TKE = (\overline{u'^2} + \overline{v'^2} + \overline{w'^2})/2))$ for the winter case. We can see large differences in TKE both along the Trombe walls on the right side of the plots as expected, since that is the location of maximum heating, and also along the left side of the figures in the vicinity of the long awnings. In addition, one can also see enhanced TKE over the roof and in the farfield above the building. When taken together with the wind fields, one would expect dispersion to be enhanced upward and along the Trombe walls and over the roof of the building. In the lee of the building, however, there may be significant subsidence, which would impact the path of potential pollutants.

A contaminant release was simulated upstream of the building and the results appear in Figure 15. One can observe enhanced spreading for the case with heating (b). The heated case generally demonstrates that the contaminant isosurface expands around the building and upward. There is a bit more contaminant spread to the left side of the plot, the region over the unheated part of the

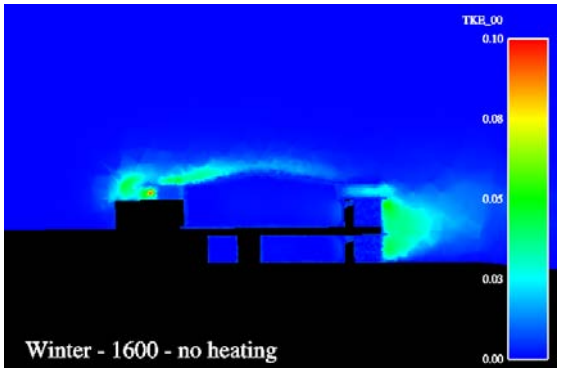

a.

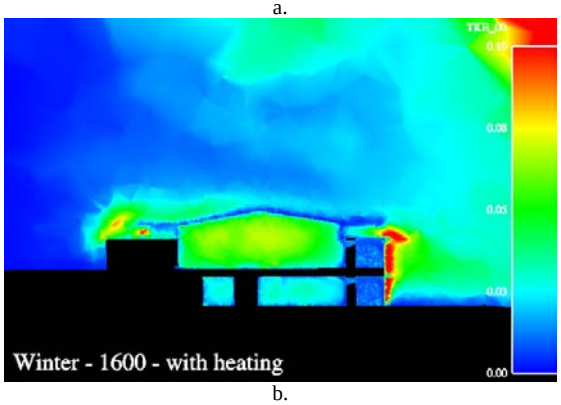

b.

Figure 14. Clip plane showing turbulent kinetic energy for a. no heating, and b. with heating for the December 1600 case.

building plus away from the building on both sides. Thus, heating does contribute to enhanced dispersion, although the differences to the field are not striking.

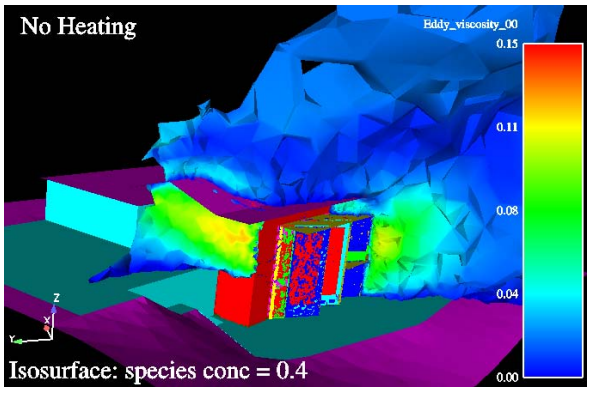

a.

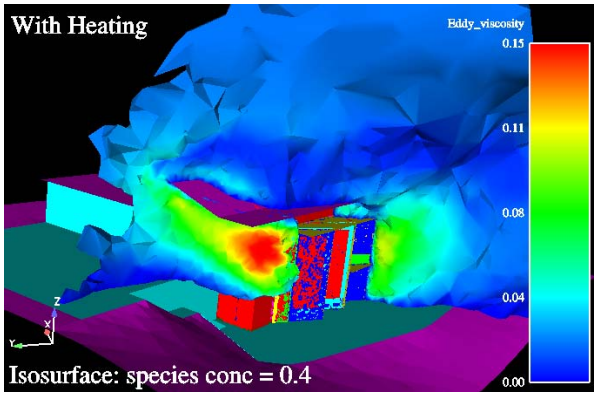

b.

Figure 15. Isosurface of contaminant colored by eddy viscosity.

IV. Discussion

In this analysis we have modeled flow features and thermal heating effects by coupling CFD to a building energy simulation model to accurately model heat transfer via convection, conduction, and radiation heat transfer. This integrated model effectively uses information on material properties, time of day, shadowing, appropriate models of transparent surfaces, and inclusion of sky radiation to iteratively compute heating and flow properties.

The test case is an environmentally friendly building that incorporates passive solar heating via large windows and Trombe walls. We have studied three different solar heating cases and compared them to a case with no heat transfer. These coupled models produce a realistic natural ventilation pattern, both internally and externally. Internal circulation is dominated by heating induced buoyancy patterns, particularly around the Trombe walls. The external circulation also demonstrates some buoyant convection due to heating. There is somewhat more convection from the roof and around the Trombe walls in the heated cases, particularly in winter when differential heating is most distinct. Note that including ceiling fans in the building design will alleviate the observed strong temperature stratification.

This work is a single case study for an isolated building. It indicates that including heat transfer mechanisms in the flow simulation modifies the fine scale structure of flow about and inside a building. Application to other buildings could display somewhat different results. The impact on contaminant dispersion outside the building is minimal. Other buildings could produce somewhat different results. An array of buildings might show different characteristics. We believe further work in this direction is merited to investigate the impact of heating on dispersion.

Acknowledgment

The authors thank Joshua Gassman and Vikram Sami of Lord, Aeck, and Sargent Architecture and John Shaw of Newcomb and Boyd Consultants and Engineers. Part of the work was funded by Penn State Applied Research Laboratory internal funds.

References

[1] Zhai Z, "Application of Computational Fluid Dynamics in building design: Aspects and trends," *Indoor Built Environ*, 15, 305-313, 2006.

[2] Tuluca A, "Visualizing how buildings breathe," *Architecture Week*. 0124, 2001.

[3] Lomas KJ, Eppel H, Martin CJ, Bloomfield DP, "Empirical validation of building energy simulation programs," *Energy and Buildings*, 26, 253-275, 1997.

[4] Zhai Z, Chen Q, Haves P, Klems JH, "On approaches to couple energy simulation and computational fluid dynamics programs," *Building and Environment*, 37, 857-864, 2002.

[5] Bartak M, Beausoleil-Morrison I, Clarke JA, Denev J, Drkal F, Lain M, Macdonald IA, Melikov A, Popiolik Z,

Stankov P, "Integrating CFD and building simulation," *Building and Environment*, 37, 865-871, 2002.

[6] Zhai Z, Chen ZY, "Numerical determination and treatment of convective heat transfer coefficient in the coupled building energy and CFD simulation," *Building and Environment*, 39, 1001-1009, 2004.

[9] Lin Y, Zmeureanu R, "Computer model of the airflow and thermal phenomena inside a large dome," *Energy and Buildings*, 40, 1287-1295, 2008.

[10] Manz, H. and Frank, T, "Analysis of thermal comfort near cold vertical surfaces by means of computational fluid dynamics," *Indoor and Built Environment*, 13, 233-242. 2004.

[11] Posner JD, Buchanan CR, Dunn-Rankin D, "Measurement and prediction of indoor air flow in a model room," *Energy and Buildings*,35, 515-526, 2003.

[12] Liping W, Wong NH, "Coupled simulations for naturally ventilated rooms between building simulation (BS) and computational fluid dynamics (CFD) for better prediction of indoor thermal environment," *Building and Environment*, 44, 95-112, 2008.

[13] Liping W, Wong NH, "Coupled simulations for naturally ventilated residential buildings," *Automation in Construction*, 17, 366-398, 2007.

[14] Yamada T, "Numerical simulations of air flows in and around a city in a coastal region," Proceedings of the Sixth Conference on Coastal Atmospheric and Oceanic Processes, San Diego, paper 5.6, 2005.

[15] Huang H, Ooka R, Kato S, "Urban thermal environment measurements and numerical simulation for an actual complex urban area covering a large district heating and cooling system in summer," *Atmospheric Env*, 39, 6362-6375, 2005.

[16] Long, K.J., F.J. Zajaczkowski, S.E. Haupt, and L.J. Peltier, "Modeling a Hypothetical Chlorine Release on a College Campus," *Journal of Computers*, 40, 881-890, 2009.

[17] Van Doormal JP, Raithby GD, "Enhancements of the SIMPLE Method for Predicting Incompressible Fluid Flows," *Numerical Heat Transfer*, **7,** 147-163, 1984.

[18] Kunz RF, Venkateswaran S, "On the Roles of Implicitness, Realizability, Boundary Conditions and Artificial Dissipation in Multidimensional Two-Fluid Simulations with Interfacial Forces," AMIF-ESF Workshop on Computing Methods for Two-Phase Flow, Centre Paul Langevin, Aussois, France, 12-14, 2000.

[19] Kunz RF, Yu WS, Antal SP, Ettorre SM, "An Unstructured Two-fluid Method Based on the Coupled Phasic Exchange Algorithm," AIAA Paper 2001-2672, 2001.

[20] Meng JCS, Uhlman JS, "Microbubble Formation and Splitting in a Turbulent Boundary Layer for Turbulence Reduction," Proceedings of the International Symposium on Seawater Drag Reduction, Newport, RI, 341-355, 1998.

[21] Thermoanalytics: RadTherm Technical Bulletins: 330: RadTherm transient CFD input. http://www.thermoanalytics.com/support/bulletins/bulletin330/index.htm. and 340: RadTherm's Convection Options, http://www.thermoanalytics.com/support/bulletins/bulletin340/index.html. 2005. (accessed 10/18/05).

[22]National Renewable Energy Laboratory: Typical Meteorological Year Database (TMY2), http://rredc.nrel.gov/solar/old_data/nsrdb/tmy2/, 2005 (accessed 4/20/05).